American Mineralogist, Volume 83, pages 590–606, 1998

Crystal structure-crystal chemistry relationships in the zeolites erionite and offretite

A. GUALTIERI,[1] G. ARTIOLI,[2,]* E. PASSAGLIA,[1] S. BIGI,[1] A. VIANI,[1] AND J.C. HANSON[3]

[1]Dipartimento di Scienze della Terra, Università di Modena, via S. Eufemia 19, I-41100 Modena, Italy
[2]Dipartimento di Scienze della Terra, Università di Milano, via Botticelli 23, I-20133 Milano, Italy
[3]Chemistry Department, Brookhaven National Laboratory, Upton, New York 11973, U.S.A.

ABSTRACT

This study clarifies the crystal structure variations and relationships in the zeolites erionite and offretite. The crystal structure analyses used Rietveld analysis of X-ray powder diffraction data, obtained both by synchrotron radiation and conventional X-ray sources, and on diffraction patterns obtained by transmission electron microscopy. The framework Al atoms in erionite are preferentially located in the single six-membered ring of tetrahedra (T2 site), whereas the Si-Al distribution is essentially disordered on the tetrahedral framework sites in offretite. In both zeolites, the center of the cancrinite cage is always occupied by K cations in similar amounts in both minerals. The erionite cage in erionite is occupied by Ca and Na atoms distributed on four distinct cation sites. Mg ions can be present up to 0.8 atoms per cell and are located between the Ca1 and Ca3 sites and very close to the Ca2 site on the symmetry axis. In offretite, the Mg site is located on the trigonal axis of the gmelinite cage and the Mg atoms are bonded to a variable number (five or six) of H_2O molecules, depending on the site population. The structural data and TEM analysis clearly show that the crystal chemistry of the extraframework cations, Mg in particular, is a major factor controlling whether erionite or offretite crystallizes, the Si-Al distribution in the framework, and the possible stacking intergrowths of the two minerals.

INTRODUCTION

Erionite and offretite are two natural zeolites of the so-called ABC-6 family (Gottardi and Galli 1985) whose members all have a topology of framework tetrahedra based on different stacking of the $4^2 \cdot 6 \cdot 8$ two-dimensional net (Smith and Bennett 1981; Millward et al. 1985). Erionite (ERI) has an average formula $Na_2K_2Ca_3[Al_{10}Si_{26}O_{72}] \cdot 30H_2O$ and is hexagonal, with space group symmetry $P6_3/mmc$ and unit-cell parameters $a \approx 13.15$, $c \approx 15.05$ Å. Offretite [OFF] has a formula $KCaMg[Al_5Si_{13}O_{36}] \cdot 16H_2O$, is hexagonal with space group symmetry $P\bar{6}m2$, and unit-cell parameters $a \approx 13.30$ and $c \approx 7.60$ Å. The framework of both zeolites is composed of columns of cancrinite cages (Staples and Gard 1959; Gard and Tait 1972) connected by a double six-membered ring of tetrahedra (hexagonal prism). The cancrinite cages (or ϵ-cages) are all similarly oriented in offretite whereas they are alternatively rotated by 60° in erionite. Adjacent columns are linked by single six-membered rings connecting cancrinite cages at the same level, forming the larger cages distinctive of each topology: offretite has gmelinite cages (or 14-hedrons) and wide channels parallel to the *c* axis delimited by 12-membered rings; erionite has large cages (erionite cages, or 23-hedrons) with the larger openings formed by eight-membered rings. In terms of six-membered rings stacking sequence along *c*, erionite, and offretite have an ·AABAAC· and an ·AAB· periodicity, respectively. The lack of six-membered rings in the *C* sequence position is the reason for the larger pores in the offretite structure.

Previous structural refinements of erionite indicate that the cancrinite cages are occupied primarily by K, and the erionite cages are occupied by Na, Ca, and Mg distributed on several cation positions located on the symmetry axis and by H_2O molecules (Kawahara and Curien 1969; Gard and Tait 1973). Cation sites may also be present near the eight-membered ring shared by two erionite cages, and these sites have been interpreted as being occupied by Na and Ca atoms (Gard and Tait 1973), though a peculiar internal exchange process between the latter cation position and the K site within the cancrinite cage has been observed in dehydrated erionite (Schlenker et al. 1977).

In offretite, the cancrinite cages are also occupied primarily by K, the gmelinite cages are occupied by Mg and H_2O molecules, and the axial positions in the large channels delimited by 12-membered rings have several sites for Na and Ca (Bennett and Gard 1967; Gard and Tait 1972). The cation position near the eight-membered rings connecting the gmelinite cage to the main structural channel seems to be largely unoccupied, though partial occupancy by K has been observed in a dehydrated offretite, as the result of internal cation exchange (Mortier et al. 1976a). The presence of a small amount of Ca has been observed inside the hexagonal prisms (or double

* E-mail: artioli@iummix.terra.unimi.it

0003–004X/98/0506–0590$05.00

TABLE 1. Occurrence and chemical composition

Locality	Chemical formula*	Si (Si + Al)	Mg (Ca + Na)
	Erionite		
Lady Hill	$Na_{0.21}K_{2.24}Mg_{0.03}Ca_{4.25}(Al_{11.03}Si_{24.97}O_{72})\cdot 36.36H_2O$	0.69	0.01
Nizhnyaya Tunguska	$Na_{0.06}K_{1.69}Mg_{0.07}Ca_{3.77}(Al_{9.60}Si_{26.41}O_{72})\cdot 31.63H_2O$	0.73	0.02
Shourdo	$Na_{0.15}K_{2.02}Mg_{0.53}Ca_{2.42}(Al_{8.51}Si_{27.59}O_{72})\cdot 28.86H_2O$	0.76	0.21
Araules	$Na_{0.03}K_{2.18}Mg_{0.83}Ca_{3.72}(Al_{11.42}Si_{24.54}O_{72})\cdot 33.57H_2O$	0.68	0.22
Agate Beach	$Na_{0.18}K_{1.77}Mg_{0.82}Ca_{2.42}(Al_{8.92}Si_{27.18}O_{72})\cdot 29.82H_2O$	0.75	0.31
	Offretite		
Fittà2	$K_{0.79}Mg_{0.70}Ca_{1.50}(Al_{5.49}Si_{12.54}O_{36})\cdot 16.72H_2O$	0.70	0.46
Fittà1	$K_{0.91}Mg_{1.02}Ca_{1.13}(Al_{5.41}Si_{12.62}O_{36})\cdot 16.64H_2O$	0.70	0.89
Mt. Semiol	$K_{0.88}Mg_{1.06}Ca_{0.97}(Al_{5.26}Si_{12.81}O_{36})\cdot 16.85H_2O$	0.71	1.09

* Passagalia et al. (1998).

six-membered rings) of offretite (Gard and Tait 1972), and it is interesting to note that the prisms contain no extraframework species in erionite. However, in related structures of the [LTL]-type, such building units are known to contain monovalent cations or H_2O molecules (Barrer and Villiger 1969; Artioli and Kvick 1990).

The accompanying paper on the crystal chemistry of erionite and offretite (Passaglia et al. 1998) shows that the two zeolites have a K content always very close to the amount required for full occupancy of the cancrinite cage (i.e., two atoms per cell in erionite and one atom per cell in offretite). Species discrimination is possible on the basis of the extraframework Mg/(Ca+Na) ratio, which is lower than 0.15 in most erionites and between 0.7–1.1 in most offretites. Previously assumed parameters for offretite and erionite discrimination, such as the tetrahedral Si/Al ratio or the optic sign of elongation (Sheppard and Gude 1969; Wise and Tschernich 1976; Gude and Sheppard 1981) are shown to be misleading and have often resulted in misidentification of mineral specimens.

A few of the studied samples show anomalous crystal chemistry: four erionite samples were found to be Ca-poor and Mg-rich [Mg/(Ca+Na) ratio between 0.20 and 0.30] and two offretite samples are rather Ca-rich and Mg-poor [Mg/(Ca+Na) ratio between 0.45 and 0.50]. Because erionite-offretite epitaxial intergrowths have been described in the literature (Bennett and Grose 1978; Passaglia et al. 1998), the borderline chemistry of these samples may be due to the presence of disordered offretite-erionite stacking sequences.

The present investigation attempts to: (1) characterize in detail the crystal structure of a few erionite and offretite samples with ''ideal'' chemical composition; and (2) define the nature of a few chemically anomalous samples, which lie between the offretite and erionite fields in the Mg-(Ca+Na)-K diagram. The present investigation utilizes the results of the recent work of Alberti et al. (1996) and Alberti et al. (1997), presenting detailed models of the offretite and erionite structures on the basis of single-crystal diffraction data.

Five erionite and three offretite samples were selected for study by Rietveld refinement using X-ray powder diffraction data. Transmission electron microscopy (TEM) studies were also carried out on several erionite and offretite crystals to investigate stacking disorder at a local level.

SAMPLES

We examined two erionite samples having close to ''ideal composition'' from Lady Hill Quarry, Northern Ireland (courtesy of H. Foy; sample no. 4 in Passaglia et al. 1998), and from Nizhnyaya Tunguska, Russia (cited as Tunguska from now on; Belitsky and Bukin 1968; sample no. 13 in Passaglia et al. 1998); three chemically anomalous erionite samples from Shourdo, Russia (Batiashvili and Gvakhariya 1968; no. 12 in Passaglia et al. 1998), from Agate Beach, Oregon (Wise and Tschernich 1976; no. 5 in Passaglia et al. 1998), and from Araules, Ht. Loire, France (Pongiluppi 1976; no. 19 in Passaglia et al. 1998); two offretite samples having an almost ''ideal composition'' from Mt. Semiol, France (Passaglia and Tagliavini 1994; no. 9 in Passaglia et al. 1998), and from Fittà, Italy (Passaglia et al. 1996; sample Fittà1: No. 11 in Passaglia et al. 1998); and one chemically anomalous offretite sample from Fittà (sample Fittà2; no. 12 in Passaglia et al. 1998).

Table 1 reports the occurrence and the mean chemical analysis of the samples (examined in detail Passaglia et al. 1998). A ternary Mg-K-(Ca+Na) diagram (Fig. 1) shows the composition of the extraframework cations; the observed compositional fields of erionites and offretites are shown for comparison.

EXPERIMENTAL METHODS

Powder diffraction data were collected with synchrotron radiation for all samples except the Agate Beach and Araules erionites. Samples were hand ground in an agate mortar, loaded in a 0.3 mm diameter glass capillary, and packed using mechanical vibrations. The capillary was set on a standard goniometer head for data collection. A spinning motor allowed rotation of the capillary in parallel-beam transmission Debye-Scherrer geometry. The diffraction data were collected on beam-line X7B at the National Synchrotron Light Source, Brookhaven National Laboratory, U.S.A. The optics of the beam-line are described in detail by Hastings et al. (1983). The beam-line

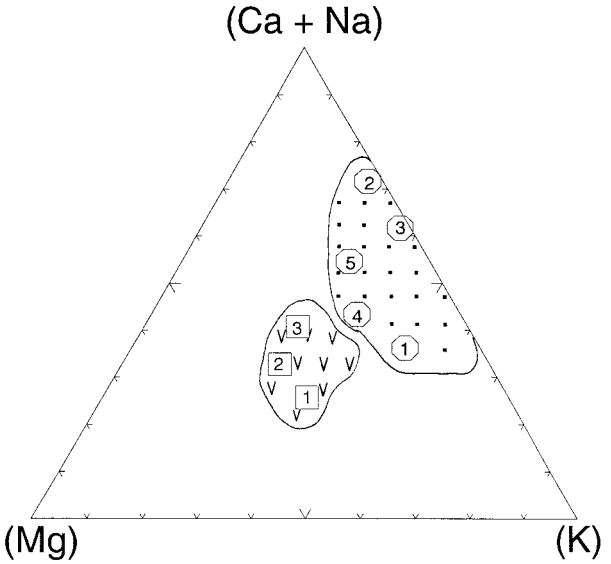

FIGURE 1. Ternary Mg-K-(Ca+Na) diagram showing the chemical content of the extraframework cation in the samples under investigation and the observed fields of erionite and offretite (modified after Passaglia et al. 1998). Open squares = offretite (1 = Mt. Semiol; 2 = Fittà1; 3 = Fittà2). Open circles = erionite (1 = Shourdo; 2 = Tunguska; 3 = Lady Hill; 4 = Agate Beach; 5 = Araules).

is equipped with a four-circle Huber diffractometer; the detector used for the data collection is a flat Imaging Plate (IP: Amemiija 1990). Standard LaB_6 (NIST SRM 660) was used for independent calibration of the experimental wavelength (0.9358 Å) in a specially developed routine that also allows the calibration of the zero-shift position of the plate, the sample-detector distance, and the tilt angle of the flat IP (Norby 1997; Gualtieri et al. 1996). The horizontal and vertical beam sizes were 1.0 and 0.3 mm, respectively. The exposure time of each diffraction image was 10 min; the data were collected in the angular range 3–60 °2θ up to $\sin\theta/\lambda = 0.53$ Å^{-1}. The virtual image stored in the plate was recovered and digitized using the Fuji BAS2000 laser scanner. Conversion from pixels to 2θ was accomplished using the parameters (sample-detector distance, zero shift, and tilt angle of the IP) determined from the refinement of standard LaB_6 peak positions. The low-2θ region (3–8°) was excluded during the refinement because of partial shadowing of the Bragg peaks in that region by the direct beam stop, resulting in anomalous intensities.

The erionite powders from the Agate Beach and Araules specimens were mounted on a flat aluminum holder and diffraction data were collected using conventional Bragg-Brentano (BB) parafocusing geometry. Cu$K\alpha$ radiation was selected using a diffracted-beam pyrolitic graphite monochromator. The data were collected in the angular range 5–140° 2θ, using steps of 0.02°, and 20 s counting time for each step. The low-2θ region (10–17°) was excluded from the refinement because the beam in this angular range was larger than the 2.0 cm long sample, causing anomalous loss of intensity (Matulis and Taylor 1992; Fischer 1996). Long counting times were employed for these samples, and diffraction peaks from the aluminum sample holder are present in the powder patterns because the available amount of powder was insufficient to fill it. The quality of these diffraction data is much lower than that of the data collected with synchrotron radiation, essentially they were used for comparison among samples.

TEM was carried out using a Philips 400T instrument operating at 100 kV and equipped with a Gatan cold stage using liquid nitrogen. Specimens were weakly hand ground in an agate mortar, suspended in ethanol, and deposited on a coated amorphous carbon film supported on a 200-mesh Cu grid. Great care was employed to minimize the effects of beam damage on the zeolite, because erionite and offretite are extremely sensitive to the electron beam and rapidly destroyed on irradiation. Selected-area electron diffraction (SAED) patterns were collected at −170 °C to slow sample degradation under the electron beam. All SAED patterns were collected with an aperture of ~0.5 μm in diameter.

REFINEMENT AND STRUCTURE ANALYSIS

All synchrotron and conventional X-ray powder data sets were analyzed by the Rietveld method using the GSAS software system (Larson and Von Dreele 1997). The structure factors were calculated using the formal scattering factors for neutral atoms. Starting atomic coordinates for the structure models of erionite and offretite were taken from Gard and Tait (1973) and Alberti et al. (1996), respectively.

The background profile was successfully fitted with a Chebyshev polynomial function with a variable number of coefficients: 20–24 for the IP data sets, and 12 for the BB data sets. The diffraction peak profiles were modeled using a pseudo-Voigt function; two Gaussian and two Lorentzian coefficients were refined. Initially the unit-cell parameters, the phase fraction were also refined. The later stages were devoted to the refinement of the atomic coordinates, the atomic site occupancies for extraframework positions, and the isotropic atomic displacement parameters. Soft constraints on tetrahedral bond lengths were imposed and used as additional observations in the earlier stages of the refinement procedure. The weight of the constraints was progressively reduced to zero in the later stages. Difference Fourier maps were repeatedly calculated from the refined model and were useful for the location of residual electron density corresponding to extraframework cations or H_2O molecules. Interpretation of the residual density maxima was based on chemical knowledge and the coordination geometry of the site, discussed in detail below.

The total number of simultaneously refined parameters, the number of observations, and the agreement indices for the final least-squares cycles are reported in Table 2. Figure 2 shows the observed (crosses), calculated (con-

TABLE 2. Statistics on the Rietveld refinements

Sample	No. of data points	No. of Bragg reflections	No. of refined parameters	Reduced χ^2	*R*wp*	*R*(F²)†
Erionite						
Lady Hill	5129	683	95	7.1	0.032	0.094
Shourdo	5129	678	95	4.6	0.028	0.092
Tunguska	5129	718	91	2.4	0.026	0.062
Araules	6100	1801	87	11.2	0.170	0.334
Agate Beach	6100	1818	87	8.7	0.093	0.150
Offretite						
Mt. Semiol	5499	397	91	3.9	0.018	0.090
Fittà1	5499	391	91	5.2	0.025	0.096
Fittà2	5499	406	87	2.5	0.014	0.082

* $R_{wp} = [\Sigma w(F_{obs}-F_{cal})^2/\Sigma w(F_{obs})^2]^{1/2}$
† $R_F^2 = \Sigma |F^2_{obs}-F^2_{cal}|/\Sigma |F^2_{obs}|$

tinuous line), and difference curves (bottom line) of the IP patterns; Figure 3 shows analogous profiles for the BB patterns.

The Lorentzian coefficients of the pseudo-Voigt peak function refined for the Araules erionite (Lorentzian FWHM at $2\theta = 20°$ is 0.22°) are anomalously large compared with the corresponding coefficients of other erionite samples (Lorentzian FWHM at $2\theta = 20°$: Agate Beach = 0.08°; Lady Hill = 0.07°; Tunguska = 0.09°; Shourdo = 0.06°). This difference indicates substantial sample broadening effects, possibly due to structural disorder or microstrain linked to stacking defects. The nature of the disorder is discussed below on the basis of the TEM data. Because of the broad peaks and the structural complexities, the least-squares refinement of the Araules erionite structure did not converge, even with highly weighted soft or hard geometrical and chemical constraints. The best fit, shown in Figure 3a, was obtained using the structure model derived from the refinement of the Agate Beach erionite and by imposing large weights on the soft tetrahedral bond distance constraints. The refined structure model is clearly unreliable in terms of the resulting interatomic distances and of the poor fit between observed and calculated diffraction patterns (Fig. 3a, Table 2). The failure of the structure refinement is related to the high density of stacking defects present in the Araules erionite.

RESULTS

Tables 3 and 4 give results from the structure refinements. Discussion of the relationship between unit-cell parameters and chemical composition is thoroughly treated in Passaglia et al. (1998). Detailed descriptions of the structures follow.

Erionite: Framework features

Two crystallographically independent tetrahedral sites are present: One forms the double six-membered ring and the base of the cancrinite cage (T1), and the other forms the single six-membered ring and the base of the erionite cage (T2). Erionite from Lady Hill with a high content of 11.03 Al atoms per cell has mean ⟨T1-O⟩ and ⟨T2-O⟩ distances of 1.61 and 1.67 Å, respectively, (difference ⟨T1-O⟩−⟨T2-O⟩ = −0.06 Å) with a clear indication that Al is partitioned in the single six-membered ring. The other three erionite samples with lower Al contents (Table 1) show much smaller differences between the mean ⟨T-O⟩ distances of the two tetrahedral sites (⟨T1-O⟩−⟨T2-O⟩ about −0.01 Å). All differences are negative, consistent with the substantial partitioning of Al into T2 found in the Lady Hill erionite. Although a difference with absolute value of 0.01 between the mean ⟨T-O⟩ distances of the two sites appears to be too small to be significant, the calculated site occupancy factors of Al in the tetrahedra using the algorithm of Alberti and Gottardi (1988), which takes into account the mean ⟨T-O⟩ distances, the T-O-T angles, and the observed dependence of the Si-O distance on the Si-O-Si angles (according to the Hill and Gibbs 1979 relationship) is striking. The results are shown in Table 5 and appear to disprove the earlier conclusions that Al in erionite is disordered on the tetrahedral framework sites (Kawahara and Curien 1969; Gard and Tait 1973). The total framework Al content calculated from the empirical algorithm is very close to that obtained from the chemical analyses (Table 5), supporting the reliability of the procedure and the consistency of the results of the structural refinements.

Erionite: Extraframework positions

The cancrinite cage is occupied by K in all refined samples, in agreement with Gard and Tait (1973). K is bonded to six framework O atoms (O2) in a trigonal prismatic coordination (Fig. 4). The K site in the center of the cancrite cage is fully occupied in the Lady Hill and Shourdo erionites, and it is partially occupied in the Agate Beach and Tunguska erionites (87 and 85% occupancy factors, respectively), in good agreement with the chemical analyses (Table 1).

Several cation positions are present in the erionite cage, mostly located at different *z*/*c* height along the symmetry axis. The three sites at ⅔, ⅓, and *z* (with $z \approx 0.60$, 0.40, and 0.20, respectively), were refined using the Ca scattering factor and labeled Ca1, Ca2, and Ca3. As shown in Figure 5, Ca3 is located near the center of the erionite cage, Ca2 is near the center of the upper half of the cavity, and Ca1 is close to the center of the single six-membered ring shared by two adjacent erionite cages, forming the base of the cavity. One additional cation site was located at (½,0,0) near the eight-membered ring opening of the cage and labeled Ca4. The Ca1 and Ca2 sites present substantial scattering density in all refined erionites, whereas Ca3 and Ca4 are generally occupied at the 15% level or less. Another site located on the symmetry axis at ($z \approx 0.10$) was interpreted as the Mg site because it is appreciably occupied in the Shourdo and Agate Beach erionites, which have larger concentrations of Mg atoms (Table 1), whereas no electron density in this position is present in the difference-Fourier maps of the Lady Hill

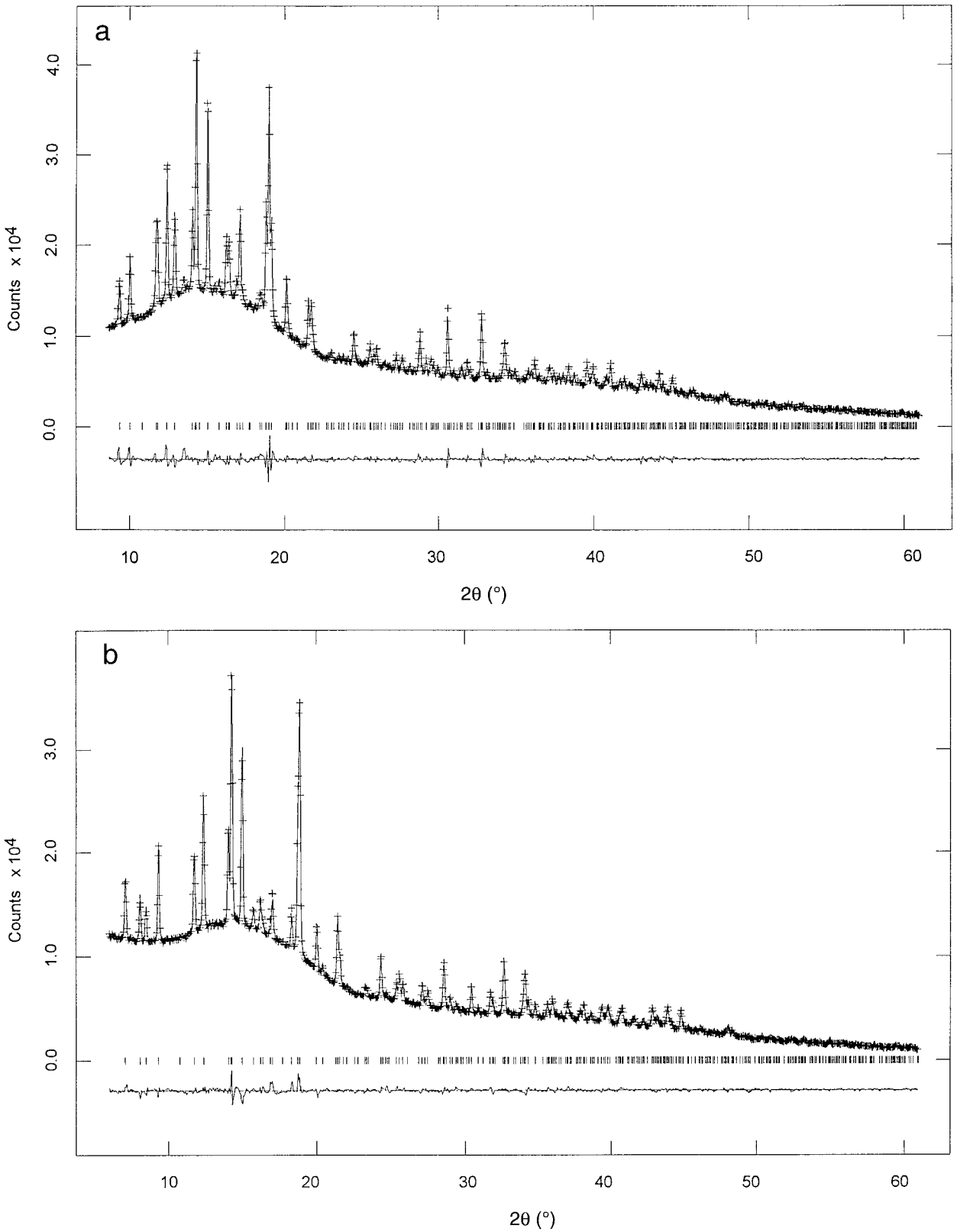

FIGURE 2. Observed (crosses), calculated (continuous line), and difference curve (bottom line) resulting from the Rietveld refinements based on the synchrotron powder patterns: (**a**) erionite from Shourdo. (**b**) offretite from Mt. Semiol.

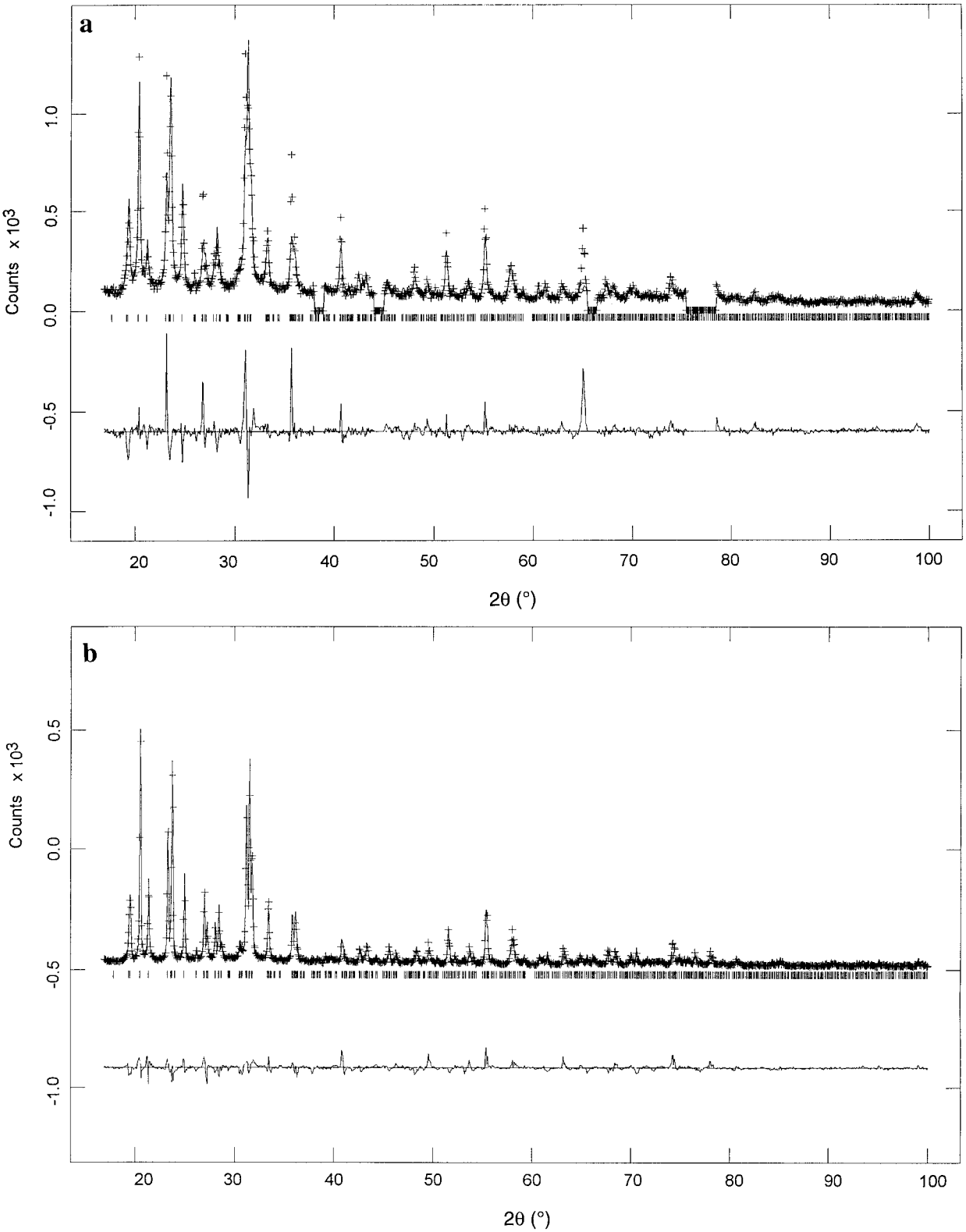

FIGURE 3. Observed (crosses), calculated (continuous line), and difference curve (bottom line) resulting from the Rietveld refinements based on the conventional powder patterns: (**a**) erionite from Araules; (**b**) erionite from Agate beach. The regions excluded from the refinement in pattern 3a contain the Al diffraction peaks from the sample holder.

TABLE 3A. Data for erionites

Site	Occupancy	Multiplicity	*x* (Å)	*y* (Å)	*z* (Å)	*U*iso (Å)
			Agate Beach [a = 13.289(1) c = 15.079(2)]			
T1	1	24	−0.0005(5)	0.2332(4)	0.1015(6)	0.031(4)
T2	1	12	0.0897(6)	0.4249(4)	0.25	0.046(4)
O1	1	24	0.0175(7)	0.3305(8)	0.1752(4)	0.057(3)
O2	1	12	0.0915(4)	0.1830(5)	0.1176(8)	0.064(5)
O3	1	12	0.1101(6)	0.2202(6)	0.6371(7)	0.062(7)
O4	1	12	0.2693(6)	0	0	0.019(5)
O5	1	6	0.2329(6)	0.4658(6)	0.25	0.088(7)
O6	1	6	0.0365(5)	0.5182(5)	0.25	0.052(5)
Ca1	0.30(3)	4	0.3333	0.6667	0.1137(8)	0.085(5)
Ca2	0.22(1)	4	0.3333	0.6667	0.9047(5)	0.079(3)
Ca3	0.16(2)	4	0.6667	0.3333	0.177(2)	0.020(4)
Mg	0.20(4)	4	0.6667	0.3333	0.049(3)	0.018(5)
K	0.87(3)	2	0	0	0.25	0.017(1)
W1	0.33(2)	12	0.245(3)	0.490(3)	0.106(2)	0.162(5)
W2b	0.86(5)	12	0.2658(9)	0.5316(9)	0.7009(8)	0.135(4)
W3	0.90(2)	12	0.422(1)	0.844(1)	0.897(3)	0.107(6)
W3b	0.30(2)	12	0.469(1)	−0.602(2)	0.073(1)	0.107(6)
W3c	0.24(2)	12	0.441(2)	0.882(2)	0.789(4)	0.107(6)
			Lady Hill [a = 13.339(1) c = 15.112(1)]			
T1	1	24	0.0012(6)	0.2308(4)	0.1058(4)	0.027(3)
T2	1	12	0.0871(5)	0.4190(6)	0.25	0.015(5)
O1	1	24	0.0295(5)	0.3443(7)	0.1584(6)	0.044(2)
O2	1	12	0.0991(5)	0.1982(6)	0.1285(7)	0.052(4)
O3	1	12	0.1266(7)	0.2532(2)	0.6284(4)	0.044(2)
O4	1	12	0.2645(5)	0	0	0.051(3)
O5	1	6	0.2314(1)	0.4628(5)	0.25	0.033(2)
O6	1	6	0.1105(3)	0.5552(6)	0.25	0.035(6)
Ca1	0.40(2)	4	0.3333	0.6667	0.118(2)	0.091(4)
Ca2	0.47(2)	4	0.3333	0.6667	0.942(1)	0.082(1)
Ca3	0.07(2)	4	0.6667	0.3333	0.221(2)	0.041(7)
Ca4	0.04(1)	6	0.5	0	0	0.091(4)
K	1	2	0	0	0.25	0.051(3)
W1	0.39(4)	12	0.2705(9)	0.5410(8)	−0.060(2)	0.067(3)
W1b	0.46(7)	12	0.2439(9)	0.4878(8)	0.0154(8)	0.067(3)
W2	0.31(4)	6	0.2050(8)	0.4100(9)	0.75	0.048(3)
W2b	0.29(5)	12	0.254(2)	0.508(5)	0.691(4)	0.048(3)
W3	0.62(5)	12	0.4414(7)	0.8828(7)	0.9141(7)	0.047(4)
W3b	0.38(6)	12	0.470(1)	−0.060(1)	0.027(2)	0.047(4)
W3c	0.18(4)	12	0.4205(9)	0.8410(8)	0.6586(8)	0.047(4)
			Shourdo [a = 13.264(1) c = 15.067(1)]			
T1	1	24	0.0006(5)	0.2329(3)	0.1052(4)	0.036(2)
T2	1	12	0.0926(3)	0.4226(7)	0.25	0.031(5)
O1	1	24	0.0251(7)	0.3473(6)	0.1609(5)	0.045(3)
O2	1	12	0.0973(5)	0.1946(6)	0.1261(7)	0.019(5)
O3	1	12	0.1263(6)	0.2526(6)	0.6320(7)	0.024(4)
O4	1	12	0.2680(5)	0	0	0.038(5)
O5	1	6	0.2310(6)	0.4620(6)	0.25	0.043(7)
O6	1	6	0.0970(3)	0.5485(3)	0.25	0.070(6)
Ca1	0.15(1)	4	0.3333	0.6667	0.104(2)	0.077(5)
Ca2	0.12(1)	4	0.3333	0.6667	0.887(1)	0.069(3)
Ca3	0.13(1)	6	0.6667	0.3333	0.2010(9)	0.032(6)
Ca4	0.14(2)	4	0.5	0	0	0.065(3)
Mg	0.13(4)	4	0.6667	0.3333	0.0730(4)	0.103(2)
K	1	2	0	0	0.25	0.038(4)
W1	0.29(5)	12	0.266(1)	0.532(1)	0.008(1)	0.086(3)
W2	0.36(6)	12	0.235(2)	0.470(2)	0.718(3)	0.128(4)
W2b	0.18(4)	12	0.260(2)	0.522(2)	0.694(3)	0.128(4)
W3	0.61(3)	12	0.431(1)	0.862(1)	0.903(2)	0.138(3)
W3b	0.22(5)	12	0.462(1)	−0.074(2)	0.029(1)	0.138(3)
W3c	0.14(7)	12	0.465(1)	0.930(1)	0.779(2)	0.138(3)
			Tunguska [a = 13.304(1) c = 15.078(2)]			
T1	1	24	0.0030(2)	0.2332(2)	0.1057(1)	0.036(4)
T2	1	12	0.0945(3)	0.4227(4)	0.25	0.028(2)
O1	1	24	0.0223(3)	0.3453(2)	0.1616(5)	0.026(1)
O2	1	12	0.0952(2)	0.1904(3)	0.1255(4)	0.042(6)
O3	1	12	0.1259(3)	0.2518(3)	0.6383(5)	0.058(2)
O4	1	12	0.2661(4)	0	0	0.040(2)
O5	1	6	0.2284(7)	0.4568(7)	0.25	0.051(2)
O6	1	6	0.0722(2)	0.5361(2)	0.25	0.061(5)

TABLE 3A—*Continued*

Site	Occupancy	Multiplicity	*x* (Å)	*y* (Å)	*z* (Å)	*U*iso (Å)
Ca1	0.16(2)	4	0.3333	0.6667	0.113(2)	0.026(4)
Ca2	0.55(3)	4	0.3333	0.6667	0.9263(9)	0.072(2)
Ca3	0.13(1)	6	0.6667	0.3333	0.219(2)	0.033(5)
Ca4	0.04(1)	4	0.5	0	0	0.095(2)
K	0.85(2)	2	0	0	0.25	0.039(3)
W1	0.39(5)	12	0.2476(9)	0.4952(9)	0.020(1)	0.128(1)
W2	0.24(4)	6	0.242(1)	0.484(1)	0.75	0.149(3)
W2b	0.46(5)	12	0.238(1)	0.476(1)	0.678(1)	0.149(3)
W3	0.74(7)	12	0.4337(9)	0.8674(9)	0.882(1)	0.128(5)
W3b	0.33(6)	12	0.534(2)	0.069(2)	0.004(1)	0.128(5)
W3c	0.19(4)	12	0.421(1)	0.842(1)	0.711(2)	0.128(5)

and Tunguska erionites, which are almost Mg-free. The cation assignment of sites Ca1 and Ca2 is in agreement with previous interpretations (Gard and Tait 1973), whereas the assignments of the Ca3 and Mg sites are reversed. Support for the present interpretation is given by the match between the overall cation content resulting from the chemical analysis (Table 1) and that recalculated from the refined site population factors. The refined cation contents are: Lady Hill = $Mg_0Ca_{4.1}$; Shourdo = $Mg_{0.5}Ca_{2.4}$; Tunguska = $Mg_0Ca_{3.6}$; Agate Beach = $Mg_{0.8}Ca_{2.7}$. The corresponding cation contents from chemical analyses, considering the total scattering power of (Ca+Na) as Ca atoms, are: Lady Hill = $Mg_0Ca_{4.4}$; Shourdo = $Mg_{0.5}Ca_{2.5}$; Tunguska = $Mg_0Ca_{3.8}$; Agate Beach = $Mg_{0.8}Ca_{2.5}$. The agreement is excellent, given the analytical uncertainties of the chemical analysis (Passaglia et al. 1998) and the complexity of the erionite Rietveld refinements. Several smaller maxima in the difference-Fourier maps were refined as H_2O molecule positions. Some of these low-occupancy sites could actually be occupied by a small amount of cations, especially Na atoms or, as in the Lady Hill erionite, by the K atoms in excess of 2.0 atoms per cell that cannot be accommodated in the cancrinite cage. Three main H_2O molecule positions were located (W1, W2, W3); in most cases they were treated as split atom sites with mutually exclusive occupancy (i.e., W1-W1b, W2-W2b, W3-W3b, or W3c).

The following discussion of the geometry of the cation sites is based on the refinement of the Lady Hill erionite, although it applies to the results of the refinements of the other erionite samples, unless specifically noted.

Ca1 is surrounded by three H_2O molecules (W1 or W1b) with bond distances in the range 2.03–2.58 Å in the different erionite samples. This position corresponds to the position $H_2O(8)$ refined by Gard and Tait (1973). The closest framework O atoms are three O5 atoms at distances in the range 3.08–3.21 Å. In the Lady Hill erionite, W1 has an alternative W1b site also connected to the Ca2 site (Ca2-W1b distance 2.34 Å). The W1b position is empty in the other samples, which contain less H_2O than the Lady Hill erionite. The H_2O molecule W1 site can be occupied only when the Ca2 and W1b sites are empty, given the very short Ca2-W1 (1.45 Å) and W1-W1b (1.29 Å) distances.

Ca2 is surrounded by nine H_2O molecule positions: three W1 or W1b sites at distances in the range 2.32–2.34 Å; three W3 (or W3c) sites at distances in the range 2.03–2.77 Å [corresponding to the $H_2O(9)$ position of Gard and Tait 1973]; and three W2 (or W2b) sites at distances in the range 2.06–2.75 Å (corresponding to the $H_2O(7)$ position of Gard and Tait 1973). The coordination number is six in the Agate Beach erionite, wherein W1 is rather distant from Ca2 (Ca2-W1 distance is 3.6 Å).

Ca3 is surrounded by several H_2O molecule positions: three W2 sites at distances in the range 2.26–2.29 Å; six W2b sites at distances in the range 2.24–2.70 Å; and six W3, W3b, or W3c sites at distances in the range 2.24–2.99 Å. Some W2b sites are closer (Ca3-W2b distances in the range 1.59–1.87 Å), but these sites are empty when Ca3 is occupied. Several W1 positions are also within bonding distance in the range 2.43–2.83 Å. However, the short H_2O-H_2O contacts (for example the short W1-W2b = 2.01 Å and W2-W2b = 1.45 Å distances) and the low-site occupancy levels indicate that the average coordination number of the Ca3 cation is six, and the H_2O molecules present at any time depend on the occupancy of the adjacent cation sites. W2b interacts by means of weak hydrogen bonds with the framework O1 atom (distances in the range 3.02–3.44 Å).

Although W2 is normally located at the intersection of the mirror plane perpendicular to [001] at $z = 0.75$ and the mirror plane perpendicular to [010] at $y = 0$, the Shourdo erionite refinement resulted in abnormally high-atomic displacement parameters for this site. A split-atom model was therefore adopted, with the H_2O molecule located off the mirror plane perpendicular to [001]. The two resulting positions are, of course, mutually exclusive.

The Ca4 site, with a low occupancy factor, is bonded to two H_2O molecules (Ca4-W3 distances in the range 1.87–2.33 Å) and to two framework O atoms (Ca4-O4 distances in the range 3.07–3.14 Å). Ca4 and W3b are not simultaneously occupied given the very short intersite distance. Ca4 is empty in the Agate Beach sample.

The position for Mg was located only in the Shourdo and Agate Beach samples, because of their appreciable Mg content. The Mg site is located between the Ca1 and Ca3 sites (at 2.66 and 1.92 Å, respectively), very close to the Ca2 site (at 0.6 Å). The short Ca-Mg distances prevent simultaneous occupation of the Mg and the Ca2, Ca3, and Ca4 cation sites. In the Shourdo erionite, the

TABLE 3B. Data for offretites

Site	Occupancy	Multiplicity	*x* (Å)	*y* (Å)	*z* (Å)	*U*iso (Å)
			Fittà1 [a = 13.390(2) c = 7.598(1)]			
T1	1	12	−0.0014(5)	0.2321(4)	0.2087(2)	0.039(3)
T2	1	6	0.0884(3)	0.4231(5)	0.5	0.020(5)
O1	1	12	0.0260(6)	0.3494(5)	0.3160(6)	0.020(5)
O2	1	6	0.0962(4)	0.9037(4)	0.2500(3)	0.028(4)
O3	1	6	0.8734(5)	0.1265(5)	0.2926(4)	0.066(4)
O4	1	6	0.0052(4)	0.2644(5)	0	0.022(5)
O5	1	3	0.2331(5)	0.7668(5)	0.5	0.026(2)
O6	1	3	0.4602(3)	0.5397(3)	0.5	0.037(4)
Ca1	0.40(6)	2	0.6667	0.3333	0.4021(7)	0.042(4)
Ca2	0.36(2)	2	0.6667	0.3333	0.2664(9)	0.048(5)
K	0.96(2)	1	0	0	0.5	0.051(5)
Mg	0.97(1)	1	0.3333	0.6667	0	0.043(3)
W1	1	2	0.3333	0.6667	0.2335(8)	0.120(4)
W2	0.81(4)	3	0.2432(7)	0.7568(7)	0	0.063(4)
W3	0.26(7)	6	0.1350(5)	0.5104(6)	0	0.060(5)
W4	0.85(4)	3	0.7663(9)	0.2337(9)	0.5	0.056(5)
W5	1	6	−0.4325(8)	0.4325(8)	0.1682(4)	0.062(6)
W6	0.32(2)	3	−0.2539(9)	0.2539(9)	0	0.060(6)
			Fittà2 [a = 13.308(3) c = 7.597(2)]			
T1	1	12	0.0006(4)	0.2317(6)	0.2048(5)	0.039(4)
T2	1	6	0.0921(5)	0.4227(6)	0.5	0.026(2)
O1	1	12	0.0208(5)	0.3479(3)	0.3173(5)	0.020(6)
O2	1	6	0.0957(4)	0.9043(4)	0.2686(3)	0.091(6)
O3	1	6	0.8761(5)	0.1239(5)	0.2900(4)	0.089(4)
O4	1	6	0.0019(4)	0.2691(6)	0	0.049(3)
O5	1	3	0.2287(5)	0.7713(5)	0.5	0.067(5)
O6	1	3	0.457(1)	0.543(1)	0.5	0.019(5)
Ca1	0.43(2)	2	0.6667	0.3333	0.3876(6)	0.041(4)
Ca2	0.32(4)	2	0.6667	0.3333	0.2438(7)	0.033(3)
K	0.89(3)	1	0	0	0.5	0.018(4)
Mg	0.86(2)	1	0.3333	0.6667	0	0.030(6)
W1	1	2	0.3333	0.6667	0.2335(8)	0.120(5)
W2	0.65(4)	3	0.2424(8)	0.7576(8)	0	0.020(5)
W3	0.55(7)	6	0.1129(5)	0.4602(6)	0	0.039(5)
W4	0.94(4)	3	0.7564(7)	0.2436(7)	0.5	0.044(6)
W5	1	6	−0.4363(6)	0.4363(6)	0.1603(8)	0.13(1)
			Mt. Semiol [a = 13.293(2) c = 7.608(1)			
T1	1	12	−0.0004(4)	0.2308(2)	0.2067(4)	0.028(3)
T2	1	6	0.0919(3)	0.4210(5)	0.5	0.030(3)
O1	1	12	0.0267(4)	0.3476(2)	0.3188(5)	0.030(5)
O2	1	6	0.0942(4)	0.9056(3)	0.2340(1)	0.016(2)
O3	1	6	0.8849(3)	0.1151(3)	0.2807(6)	0.026(2)
O4	1	6	0.0093(3)	0.2722(4)	0	0.032(7)
O5	1	3	0.2271(3)	0.7729(3)	0.5	0.010(5)
O6	1	3	0.4545(7)	0.5455(7)	0.5	0.051(5)
Ca1	0.43(3)	2	0.6667	0.3333	0.353(4)	0.067(3)
Ca2	0.27(3)	2	0.6667	0.3333	0.245(5)	0.052(3)
K	1	1	0	0	0.5	0.040(2)
Mg	1	1	0.3333	0.6667	0	0.026(5)
W1	1	2	0.3333	0.6667	0.2587(9)	0.043(4)
W2	0.80(4)	3	0.2437(8)	0.7563(7)	0	0.041(6)
W3	0.30(5)	6	0.1740(8)	0.4957(9)	0	0.060(4)
W4	1	3	0.7579(7)	0.2421(7)	0.5	0.058(4)
W5	0.35(3)	6	−0.4357(8)	0.4357(8)	0.1713(2)	0.042(6)
W5b	0.37(3)	6	−0.4820(7)	0.4820(7)	0.1231(5)	0.042(5)

Mg cation is surrounded by six H_2O molecules (three W1 at 1.91 Å and three W3 at 2.28 Å) in a distorted octahedral environment (Fig. 6). In the Agate Beach erionite, the Mg cation has a similar environment with W2b at 2.76 Å and W3 at 2.19 Å.

The total number of refined H_2O molecules is 29.7, 21.6, and 26.8 for the Lady Hill, Shourdo, and Tunguska samples, respectively. The values are all underestimated with respect to the number of H_2O molecules obtained from the TG analyses (Passaglia et al. 1998). It is likely that the undetected H_2O molecules are disordered in the erionite cages, since no refinable density maxima were found in the residual difference-Fourier maps. The number of H_2O molecules resulting from the Agate Beach refinement is 31.6, in good agreement with the TG analyses.

Concerning the framework-extraframework cation interactions, the ordering of Al in the T2 site can be nicely explained by taking into account the Ca bonding with the framework O atoms. Ca1 is bonded to three H_2O molecules in the W1 or W1b sites, and to three framework O atoms (O5). As the cation population of the Ca1 site in-

TABLE 4A. Selected bond lengths (Å) and bond angles (°) for erionite

Agate Beach			
T1-O1	1.629(2)	T2-O1×2	1.600(1)
T1-O2	1.677(1)	T2-O5	1.697(2)
T1-O3	1.644(2)	T2-O6	1.706(3)
T1-O4	1.602(3)		
mean T1-O	1.638(3)	mean T2-O	1.650(2)
T1-O1-T2	153.5(3)		
T1-O2-T1	136.1(2)		
T1-O3-T1	140.2(4)		
T1-O4-T1	145.4(5)		
T2-O5-T2	147.8(3)		
T2-O6-T2	137.9(6)		
Ca1-O5×3	3.09(2)	K-O2×6	2.90(2)
Ca1-W1×3	2.03(1)		
Ca1-Mg	2.45(2)	Mg-W2b×3	2.76(3)
		Mg-W3×3	2.19(4)
Ca2-W2b×3	2.22(2)		
Ca2-W3×3	2.04(2)	W2b-W2b	1.48(3)
Ca2-W3c×3	3.03(1)	W2b-W3×2	2.17(2)
Ca2-Ca3	1.23(3)	W2b-W3c×2	2.17(1)
Ca2-Mg	0.690(3)		
		W3-W2b×2	2.17(2)
Ca3-W2b×3	1.59(3)	W3-W3b×2	1.39(3)
Ca3-W2b×3	2.40(2)	W3-W3c	1.68(2)
Ca3-W3×3	2.32(3)		
Ca3-W3c×3	2.53(2)	W3b-W3b	1.76(2)
Ca3-W3c×3	2.99(1)		
Ca3-Mg	1.93(7)	W3c-O6	1.87(5)
Ca3-Ca3	2.20(2)	W3c-W3c	1.17(3)
Lady Hill			
T1-O1	1.580(2)	T2-O1×2	1.652(3)
T1-O2	1.606(2)	T2-O5	1.709(3)
T1-O3	1.608(1)	T2-O6	1.683(4)
T1-O4	1.663(2)		
mean T1-O	1.614(2)	mean T2-O	1.674(4)
T1-O1-T2	144.6(3)		
T1-O2-T1	142.9(4)		
T1-O3-T1	148.3(5)		
T1-O4-T1	148.0(4)		
T2-O5-T2	145.6(6)		
T2-O6-T2	161.5(4)		
Ca1-O5×3	3.08(2)	Ca4-O4×2	3.14(1)
Ca1-W1×3	3.06(2)	Ca4-W3×2	1.87(3)
Ca1-W1b×3	2.58(2)	Ca4-W3b×2	0.80(3)
Ca1-Ca2	2.66(5)	Ca4-W3c×2	3.02(2)
Ca2-W1×3	1.45(2)	K-O2×6	3.00(9)
Ca2-W1b×3	2.34(1)		
Ca2-W2b×3	2.71(6)	W1-W1b	1.29(3)
Ca2-W3×3	2.53(4)	W1-W2b	2.01(6)
Ca2-W3c×3	2.52(1)		
Ca2-Ca4	2.47(3)	W2-W2b×2	1.45(6)
Ca3-W1×3	2.83(1)	W2b-W2b	1.78(1)
Ca3-W2×3	2.99(1)	W2b-W3c×2	1.98(2)
Ca3-W2b×3	1.87(3)		
Ca3-W2b×3	2.24(2)	W3-W3b	1.82(3)
Ca3-W3c×3	2.24(1)	W3-W3c	1.20(5)
Ca3-W3c×3	2.71(2)		
		W3b-W3b	1.61(6)
		W3c-W3c	1.20(3)
Shourdo			
T1-O1	1.619(2)	T2-O1×2	1.644(2)
T1-O2	1.628(2)	T2-O5	1.638(3)
T1-O3	1.608(3)	T2-O6	1.641(2)
T1-O4	1.653(3)		
mean T1-O	1.629(3)	mean T2-O	1.641(3)
T1-O1-T2	141.7(2)		
T1-O2-T1	141.2(4)		
T1-O3-T1	146.3(4)		
T1-O4-T1	146.9(3)		
T2-O5-T2	147.8(5)		
T2-O6-T2	176.4(4)		

TABLE 4A—*Continued*

Ca1-W1×3	2.18(3)	Ca4-O4×2	3.07(1)
Ca1-W3b×3	3.18(3)	Ca4-W3×2	2.14(4)
Ca1-Mg	2.66(4)	Ca4-W3b×2	0.96(2)
Ca1-O5×3	3.21(2)		
		K-O2×6	2.913(6)
Ca2-W1×3	2.32(5)		
Ca2-W2×3	2.75(1)	Mg-W1×3	1.91(3)
Ca2-W2b×3	2.06(1)	Mg-W2b×3	2.47(1)
Ca2-W3×3	2.26(4)	Mg-W3×3	2.28(4)
Ca2-Ca3	1.32(6)		
Ca2-Mg	0.60(6)	W2-W2	0.95(1)
		W2-W2b	1.44(1)
Ca3-W2×3	2.26(5)	W2-W2b	0.68(8)
Ca3-W2×3	2.56(3)		
Ca3-W2b×3	1.67(3)	W2b-W2b	1.68(1)
Ca3-W2b×3	2.29(2)	W3-W3b	2.03(5)
Ca3-W3×3	2.74(6)	W3-W3c	2.03(1)
Ca3-Mg	1.92(1)		
Ca3-Ca3	1.47(1)		
		W3b-W3b	1.92(6)
		W3c-W3c	0.86(6)
		W3c-O6	1.96(6)
Tunguska			
T1-O1	1.618(2)	T2-O1×2	1.664(2)
T1-O2	1.612(2)	T2-O5	1.602(2)
T1-O3	1.665(3)	T2-O6	1.677(3)
T1-O4	1.658(1)		
mean T1-O	1.639(2)	mean T2-O	1.652(3)
T1-O1-T2	139.7(2)		
T1-O2-T1	138.1(1)		
T1-O3-T1	141.3(3)		
T1-O4-T1	149.1(3)		
T2-O5-T2	151.4(4)		
T2-O6-T2	162.3(3)		
Ca1-O5×3	3.17(2)	Ca4-O4×2	3.11(1)
Ca1-W1×3	2.41(2)	Ca4-W3×2	2.33(2)
Ca1-Ca3	2.81(3)	Ca4-W3b×2	0.79(2)
Ca2-W2×3	2.14(1)	K-O2×6	2.898(9)
Ca2-W2b×3	2.27(2)		
Ca2-W2b×3	2.67(2)	W2-W2b	1.07(3)
Ca2-W3×3	2.77(2)	W2-W3c	2.14(2)
Ca2-W3c×3	2.03(1)		
Ca2-W3c×3	2.28(2)	W2b-W2b	2.14(3)
Ca2-Ca3	3.11(1)	W2b-W3c×2	2.16(5)
Ca3-W1×3	2.43(1)	W3-W3b	1.85(8)
Ca3-W2b×3	2.70(2)	W3-W3c	1.44(4)
Ca3-W3×3	2.40(3)		
Ca3-W3c×3	2.90(2)	W3b-W3b	1.59(6)
		W3c-W3c	1.17(3)

creases (from 0.15 in Shourdo to 0.40 in Lady Hill), the Ca1-O5 distance decreases (from 3.21 Å in Shourdo to 3.08 Å in Lady Hill). Because the increase in the population of Ca1 shortens the Ca1-O5 distances, the adjacent T2 sites are preferentially occupied by Al in place of Si, to compensate for the charge saturation of the O5 atoms. Ca3, which is also bonded to a few O4 atoms, which in turn are connected to T1 atoms, shows a very low population in all our refinements and thus it has a very minor influence on the Si-Al distribution.

Offretite: Framework features

Two crystallographically independent tetrahedral sites were refined: T1 forming the double six-membered rings, and T2 forming the single six-membered rings. The Mt. Semiol sample has a mean ⟨T1-O⟩ distance of 1.638 Å and a mean ⟨T2-O⟩ distance of 1.650 Å. In the Fittà1 sample, the mean ⟨T1-O⟩ distance is 1.650 Å and the ⟨T2-

TABLE 4B. Selected bond lengths (Å) and bond angles (°) for offretites

		Fittà1	
T1-O1	1.632(2)	T2-O1×2	1.670(1)
T1-O2	1.659(1)	T2-O5	1.712(1)
T1-O3	1.677(2)	T2-O6	1.614(1)
T1-O4	1.633(2)		
mean T1-O	1.650(2)	mean T2-O	1.666(1)
T1-O1-T2	141.4(2)		
T1-O2-T1	140.9(3)		
T1-O3-T1	132.4(5)		
T1-O4-T1	152.1(2)		
T2-O5-T2	146.6(5)		
T2-O6-T2	177.7(5)		
Ca1-W4×3	2.41(3)	K-O2×6	2.92(2)
Ca1-W5×3	2.89(2)	K-O3×6	3.31(3)
Ca1-Ca1	1.48(5)		
Ca1-Ca2	1.03(6)	Mg-W1×2	2.00(3)
Ca1-Ca2	2.51(2)	Mg-W2×3	2.07(3)
		Mg-W3×6	2.40(6)
Ca2-W4×3	2.90(2)		
Ca2-W5×3	2.40(2)	W2-W3×2	1.62(3)
Ca2-W6×3	2.72(4)		
		W3-W3	1.51(4)
		Fittà2	
T1-O1	1.667(1)	T2-O1×2	1.694(2)
T1-O2	1.673(1)	T2-O5	1.636(1)
T1-O3	1.687(1)	T2-O6	1.642(2)
T1-O4	1.631(1)		
mean T1-O	1.664(2)	mean T2-O	1.666(2)
T1-O1-T2	138.4(2)		
T1-O2-T1	132.7(2)		
T1-O3-T1	132.7(4)		
T1-O4-T1	145.0(3)		
T2-O5-T2	151.7(5)		
T2-O6-T2	174.9(4)		
Ca1-W4×3	2.23(3)	K-O2×6	2.82(3)
Ca1-W5×3	2.93(5)	K-O3×6	3.27(2)
Ca1-Ca1	1.70(4)		
Ca1-Ca2	1.09(3)	Mg-W1×2	2.07(2)
Ca1-Ca2	2.80(5)	Mg-W2×3	2.09(1)
		Mg-W3×6	2.84(2)
Ca2-W4×3	2.84(3)		
Ca2-W5×3	2.45(1)	W2-W3×2	1.58(3)
		W3-W3	1.51(4)
		Mt. Semiol	
T1-O1	1.645(2)	T2-O1×2	1.660(2)
T1-O2	1.629(1)	T2-O5	1.623(3)
T1-O3	1.631(2)	T2-O6	1.660(1)
T1-O4	1.650(2)		
mean T1-O	1.638(1)	mean T2-O	1.650(1)
T1-O1-T2	142.0(3)		
T1-O2-T1	142.1(5)		
T1-O3-T1	139.6(3)		
T1-O4-T1	144.8(2)		
T2-O5-T2	152.8(3)		
T2-O6-T2	179.0(6)		
Ca1-W4×3	2.38(1)	Mg-W1×2	1.96(1)
Ca1-W5×3	2.73(2)	Mg-W2×3	2.06(2)
Ca1-Ca1	2.23(6)	Mg-W3×6	2.20(1)
Ca1-Ca2	0.82(2)		
		W2-W3×2	0.98(2)
Ca2-W4×3	2.86(2)		
Ca2-W5×3	2.42(2)	W3-W3	1.96(2)
		W5-W5b	
K-O2×6	2.96(2)	W5b-W5b	1.12(3)
K-O3×6	3.12(1)		1.87(4)

O⟩ distance is 1.666 Å. In the Fittà2 sample, mean ⟨T1-O⟩ and ⟨T2-O⟩ distances are 1.664 and 1.666 Å, respectively. The difference values (Fig. 7) are all very small and agree with the model of a disordered distribution of Si,Al in the tetrahedral sites of offretite as proposed by Mortier et al. (1976a, 1976b) and confirmed by Alberti et al. (1996). These results disagree with the model of ordering of Al in the T1 site by Gard and Tait (1972). Although the observed Δ⟨T-O⟩ values are small, the present results may suggest that if Si,Al ordering exists in offretite, then Al is preferentially partitioned in the T2 site rather than in T1. Furthermore, the consistent trend of Al content with Δ⟨T-O⟩ (Fig. 7) indicates that a decrease in total Al content of the structure is related to an increase in partitioning of Al into the T2 site.

TABLE 5. Calculated Al content of the tetrahedral sites in erionite

Locality	|Δ(T-O)|	Al(T1)%	Al(T2)%	Total Al% EPMA*	Total Al% calculated
Lady Hill	0.060(2)	6.1	48.8	30.6	28.9
Shourdo	0.012(1)	17.7	30.5	23.6	21.9
Tunguska	0.013(1)	24.6	35.5	26.6	28.2
Agate Beach	0.012(1)	17.0	34.5	24.7	22.8

Note: The procedure of Alberti and Gottandi (1988) was used.
* Passaglia et al. (1998).

Offretite: Extraframework positions

The K cations are found exclusively in the cancrinite cage where they are bound to six framework O atoms in trigonal prismatic coordination. The refined site occupancy factors are in good agreement with the chemical analyses, even though a systematic slight overestimation of the K content from the refinement with respect to the analytical value was observed. The K site was refined as fully occupied in the Mt. Semiol offretite with a K-O(2) distance of 2.96 Å. The refinement of Fittà1 sample showed a refined population of 0.96 (analytical 0.91) and

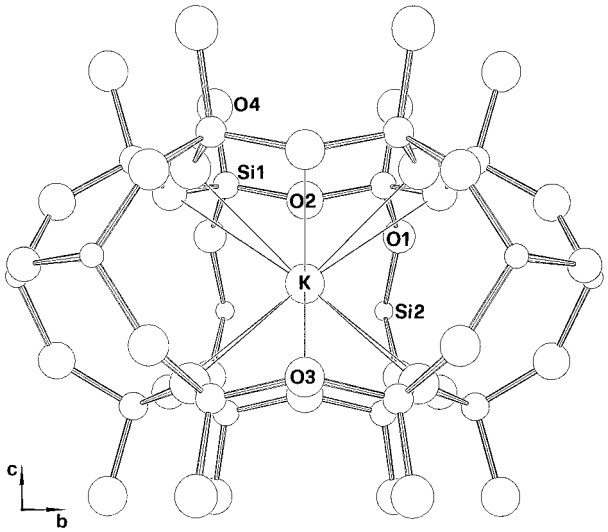

FIGURE 4. ORTEP plot of the cancrinite cage in erionite showing the interaction of K with the framework O atoms O2 (×6) and O3 (×6).

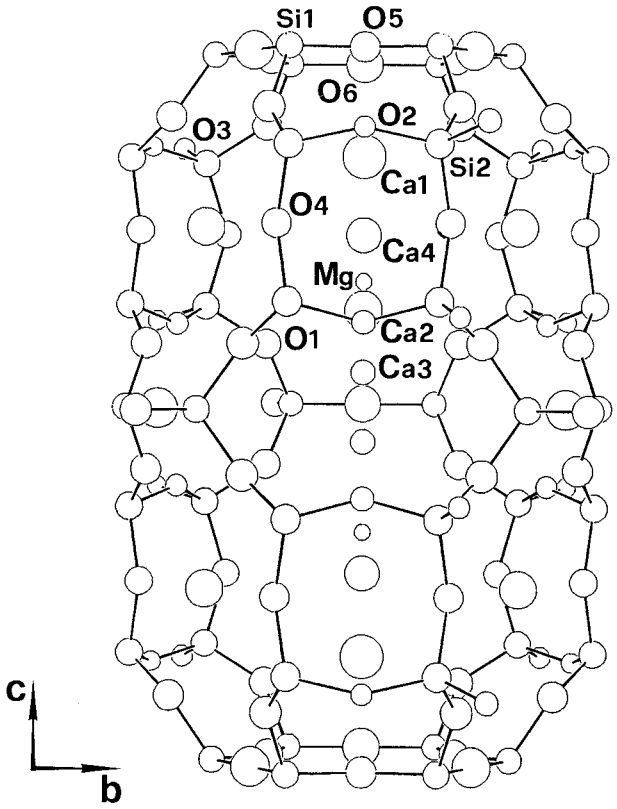

FIGURE 5. ORTEP plot of the erionite cage showing the positions of the extraframework cations. H_2O molecules are not shown for the sake of clarity.

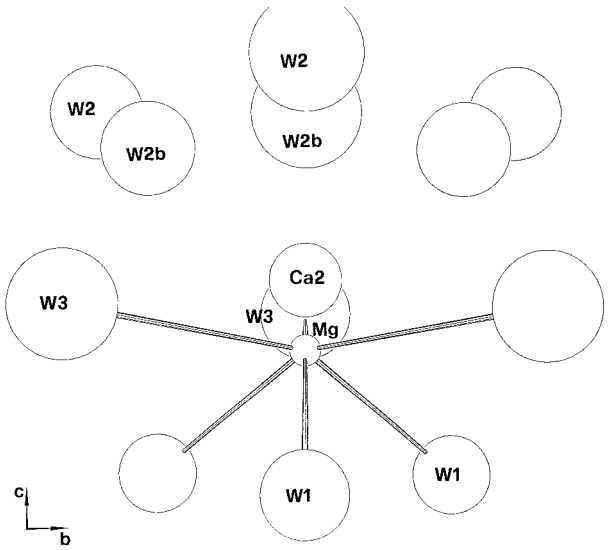

FIGURE 6. ORTEP plot of the coordination environment of Mg in the erionite cage showing the interactions with the H_2O molecules W1 and W3. The Ca2 site is shown although the Mg and Ca2 sites cannot be simultaneously occupied. The W2 and W2b H_2O molecule sites also cannot be simultaneously occupied.

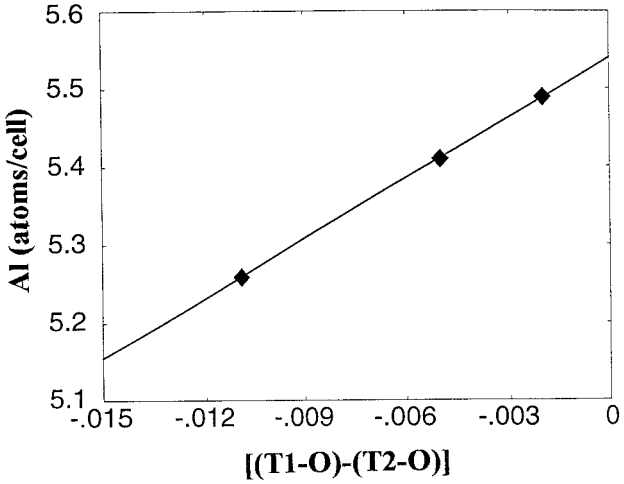

FIGURE 7. Total Al content (Al atoms per cell) vs. ⟨T1-O⟩−⟨T2-O⟩ difference values in offretites.

the K-O(2) distance of 2.92 Å. The cancrinite cage is not fully occupied in Fittà2 as well (0.89, analytical 0.79) and the K-O(2) distances are 2.82 Å.

The Mg site is on the trigonal axis in the gmelinite cage (Fig. 8) and is coordinated to a variable number of H_2O molecules depending on its occupancy factor. Alberti et al. (1996) observed that Mg is coordinated by six H_2O molecules in a more or less regular octahedral geometry for a sample with 1.1 Mg atoms per unit cell, resulting from ''two fully occupied H_2O sites placed, above and below, on the same axis (W7), and to four H_2O, which lie on a plane parallel to (0001) at the same height as Mg. Two symmetrically independent H_2O sites have been found on this plane: W8, with multiplicity three and W9, with multiplicity six.'' The proposed model involves si-

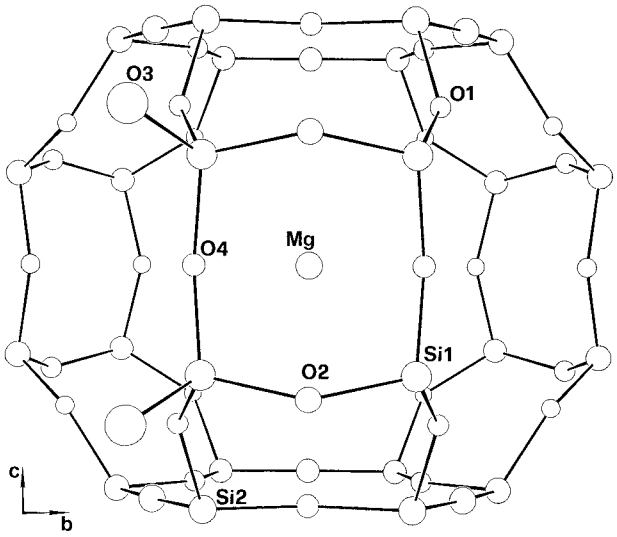

FIGURE 8. ORTEP plot of the gmelinite cage centered by Mg in offretite. H_2O molecules are not shown for clarity.

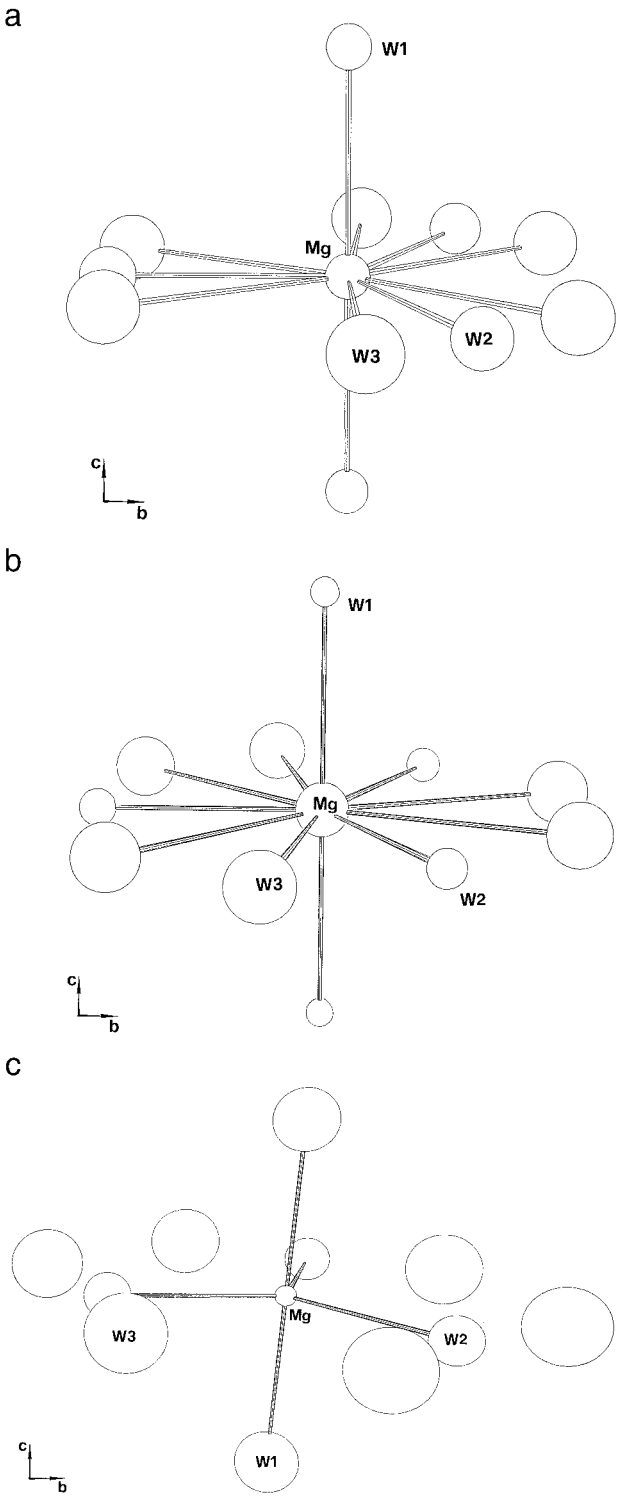

FIGURE 9. ORTEP plots of the Mg coordination environment in offretite. (**a**) offretite Mt. Semiol. Mg is bonded to two W1 at 1.96 Å, three W2 at 2.06 Å, and six W3 at 2.20 Å (W2−W3 = 0.98 Å; W3−W3 = 1.96 Å) in an octahedral environment very similar to the one reported by Alberti et al. (1996); (**b**) Fittà1 W3 is at a greater distance (Mg−W3 = 2.40 Å) in an intermediate situation between the one described by Alberti et al. (1996) and the one proposed by Gard and Tait (1972) where Mg is bonded to two W1 (2 atoms per cell) at 2.00 Å, three W2 at 2.07 Å (2.4 atoms per cell), and six W3 (1.5 atoms per cell) at 2.40 Å (W2−W3 = 1.62 Å; W3−W3 = 1.51 Å); (**c**) Fittà2 Mg coordination is close to the model proposed by Gard and Tait (1972), and Mg is bonded to two W1 (2 atoms per cell) at 2.07 Å, three W2 (2.8 atoms per cell) at 2.09 Å, and six W3 at 2.84 Å (W2−W3 = 1.58 Å). Mg is in a distorted fivefold coordination.
←

multaneous occupancy of only four out of the nine in-plane H_2O sites, implying two possible configurations: three W9 and one W8 sites or two W9 and two W8 sites. Gard and Tait (1972) also refined W7, W8, and W9 sites in their sample (having 0.7 Mg atoms per cell) but they suggested a different bonding model in which Mg has a distorted fivefold coordination of three W8 and two W7. We refined the W1, W2, and W3 positions (W7, W8, and W9, respectively, of Gard and Tait 1972) for all samples. The offretite from Mt. Semiol (with a composition close to that refined by Alberti et al. 1996): 1.1 Mg atoms per cell both from chemical analysis and from site-population refinement, the Mg cation is bonded to two W1 at 1.96 Å, three W2 at 2.06 Å, and six W3 at 2.20 Å (W2–W3 = 0.98 Å; W3–W3 = 1.96 Å) in an octahedral environment very similar to that reported by Alberti et al. (1996). We refined a population of 2.4 atoms per cell for W8 and 1.8 atoms per cell for W9, showing that a (0001) in-plane configuration of two W8 + 2W9 H_2O molecules is more likely (Fig. 9a). In the Fittà1 offretite, where the analytical Mg is ~1.0 atoms per cell (the refined value is 0.97 atoms per cell), we observed that the Mg-W3 distance is substantially longer (2.40 Å). The coordination geometry (Fig. 9b) can be described as intermediate between that described by Alberti et al. (1996) and the geometry proposed by Gard and Tait (1972) where the sixfold coordination of Mg is obtained by bonding to two W1 sites (2 atoms per cell) at 2.00 Å, three W2 sites at 2.07 Å (2.4 atoms per cell), and six W3 sites (1.5 atoms per cell) at 2.40 Å (W2-W3 = 1.62 Å; W3-W3 = 1.5 Å). The Mg coordination in the offretite from Fittà2 (having 0.7 Mg atoms per cell vs. a refined population of 0.86 Mg atoms per cell) (Fig. 9c) closely resembles the model proposed by Gard and Tait (1972). Here, Mg is bonded to two W1 (2 atoms per cell) at 2.07 Å, 3 W2 (2.8 atoms per cell) at 2.09 Å, and six W3 at 2.84 Å (W2–W3 = 1.58 Å). The Mg cation is now in a distorted fivefold coordination. Thus, the Mg content controls the number of coordinated H_2O molecules: The lower the site population, the lower the number of coordinated H_2O molecules.

Concerning the Ca atoms, two independent Ca1 and Ca2 sites were refined based on the results of the refinement by Alberti et al. (1996), implying that the Ca atoms are found at the center of the wide channel, at different heights along the trigonal axis (Fig. 10). No site was

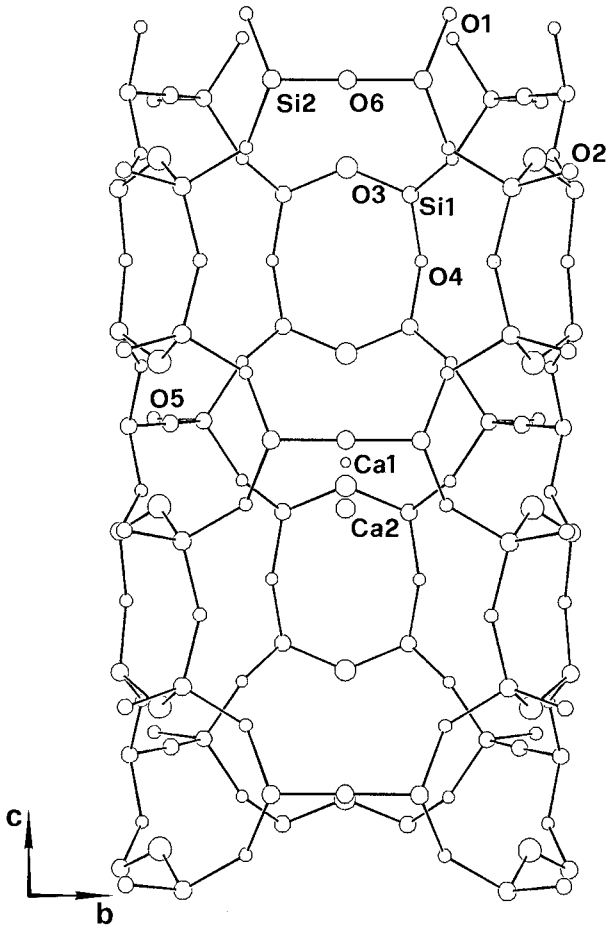

FIGURE 10. ORTEP plot of the coordination environment of Ca1 and Ca2 atoms in offretite. H_2O molecules are not reported for clarity.

found in the cavity of the double six-membered ring as reported by Gard and Tait (1972). All refinements show a refined Ca population higher than that resulting from the chemical analysis. The same result was found by Alberti et al. (1996), as they reported a refined population of 1.32 Ca atoms per cell, whereas the value from the chemical analysis is 1.07 Ca atoms per cell. In the refinement of the offretite from Mt. Semiol for example, the Ca content calculated from the refinement is 1.40 Ca atoms per cell vs. 0.97 Ca atoms per cell resulting from the electron microprobe analysis. We believe this difference may be due to cation migration during the analysis (also indicated by a large positive balance error E = 5.6%), although it is possible that some H_2O is also present in the site. The refinement results are: Mt. Semiol = $Mg_{1.0}Ca_{1.4}$; Fittà1 = $Mg_{1.0}Ca_{1.5}$; Fittà2 = $Mg_{0.9}Ca_{1.5}$; and the corresponding chemical analyses are: Mt. Semiol = $Mg_{1.1}Ca_{1.0}$; Fittà1 = $Mg_{1.0}Ca_{1.1}$; Fittà2 = $Mg_{0.7}Ca_{1.5}$.

Ca1 is surrounded by three W4 H_2O molecules (Ca1-W4 distance in the range 2.23–2.41 Å) and three W5 molecules (Ca1-W5 distance in the range 2.73–2.93 Å) in sixfold coordination. Because the Ca1-Ca2 distances are short (0.82–1.09 Å) the two sites cannot be simultaneously occupied. Ca2 is again in an octahedral environment as it is surrounded by three W4 molecules (distances of 2.84–2.90 Å) and three W5 (distances of 2.40–2.45 Å). Ca2 in Fittà1 is also weakly coordinated to three W6 molecules at 2.72 Å, possibly with ninefold coordination. According to Alberti et al. (1996), the Ca1–Ca2 distances for all our samples and the partial occupancy of the two sites could be explained by non-simultaneous occupancy of the cation sites.

Concerning the H_2O molecules, the five refined positions (W1–W5) match those found by Alberti et al. (1996) and labeled O_{W7}–O_{W11}. The refined number of H_2O molecules in the Mt. Semiol offretite is 13.6. A new site was refined on the same plane of W5 and was labeled W5′, whereas the O_{W12} site of Alberti et al. (1996) was found to be empty. The value is underestimated with respect to the H_2O content resulting from the TG (Passaglia et al. 1998). As in erionite, it is likely that the undetected molecules are disordered in the structure: No refinable density maxima were found in the difference-Fourier maps. Offretite from Fittà1 has a total number of H_2O molecules of 15.80. The O_{W12} site of Alberti et al. (1996) was also refined. The sample from Fittà2 has a total number of refined H_2O molecules of 16.16. The W6 site was not found in this sample. The values agree with the expected H_2O molecules calculated from the TG (Passaglia et al. 1998).

TEM results

Selected-area electron diffraction (SAED) patterns of the erionites from Shourdo, Tunguska, Agate Beach, and Araules, and offretites from Mt. Semiol and Fittà2 were collected to detect and characterize possible structural disorder. Samples of erionite from Lady Hill and offretite from Fittà1 were excluded from the investigation because they represent ''ideal'' stoichiometry, and thus are unlikely to contain defects and disorder. This assumption is supported by the results of the Rietveld refinement.

Crystals were oriented using the double tilt of the sample stage such that the reciprocal lattice planes containing the c^* axis were displayed. This orientation is used to distinguish between the two structures because the c axis is doubled in erionite and permits evaluation of the presence of planar defects in the stacking sequences of intergrowths (Kerr et al. 1970; Bennett and Grose 1978). The cancrinite cages in Mg-rich erionites may to a certain extent be rotated 60° counterclockwise to generate offretite sequences. The many collected SAED patterns of erionite crystals from Shourdo, Tunguska, and Agate Beach consistently displayed sharp diffraction spots. Examples are reported in Figure 11. Offretite can occur in erionite as individual microcrystals (i.e., a few large offretite domains: Kokotailo et al. 1972) or as isolated stacking faults (i.e., many small offretite domains: Kerr et al. 1970; Bennett and Grose 1978). The first effect alters the diffraction intensities at a macroscopic level, and it is easily detect-

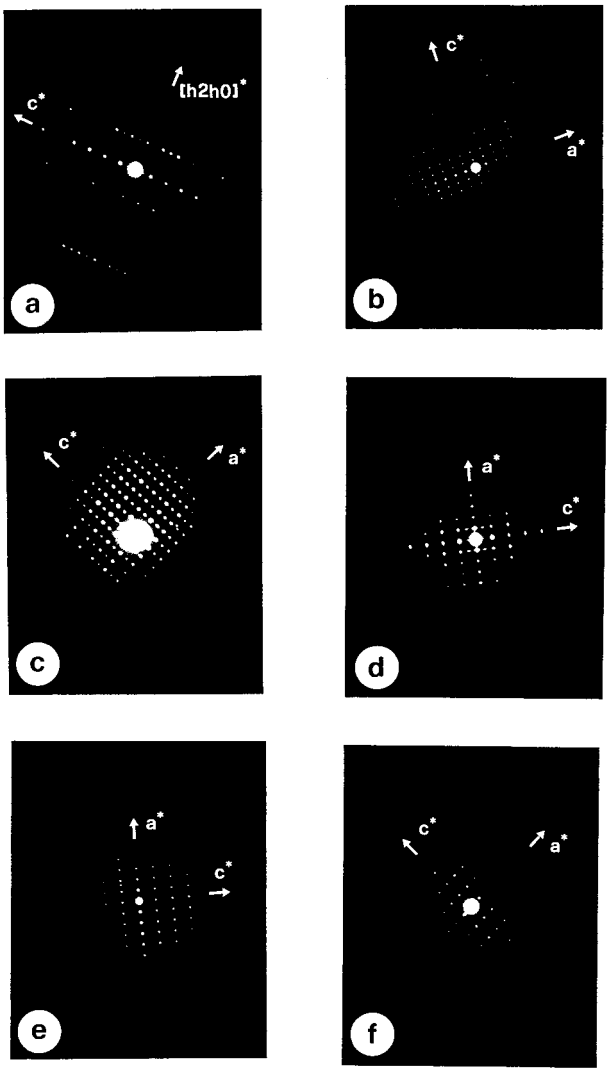

FIGURE 11. SAED patterns: (**a**) [$2\bar{1}\bar{1}0$] zone axis, erionite from Shourdo; (**b**) [$01\bar{1}0$] zone axis, erionite from Tunguska; (**c**) [$01\bar{1}0$] zone axis, erionite from Agate Beach; (**d**) [$2\bar{1}\bar{1}0$] zone axis, erionite from Araules; (**e**) [$2\bar{1}\bar{1}0$] zone axis, offretite from Mt. Semiol; (**f**) [$01\bar{1}0$] zone axis, offretite from Fittà1.

able in the X-ray diffraction patterns (Passaglia et al. 1998). The second effect is more easily seen by electron diffraction, because if the density of stacking faults is substantial, then an appreciable broadened or streaked intensity appears at the position of the odd *l* reflections, which are sharp in pure unfaulted erionite. The absence of diffuse intensity or streaks parallel to the [0001] direction indicates that the crystal contains no faults in the stacking sequence. Diffraction spots 000*l* with $l = 2n + 1$ in the [000l]* rows of all erionite samples apparently break the conditions imposed by the systematic absences for that space group, but this is a physical effect due to multiple diffraction effects from a thick section of the specimen under the beam.

Figure 11d is a representative SAED pattern of the erionite crystals from Araules. Diffraction spots with *l* odd that belong to the [$10\bar{1}$l] and [$\bar{1}01$l] reciprocal lattice rows are streaked in the direction parallel to *c** indicating that highly defective erionite-offretite stacking sequence occurs. Disorder affects domains as long as ~300 erionite unit cells. SAED patterns of offretite samples (Figs. 11e and 11f) show well-defined spots and total absence of intensity at the odd *l* reflections, indicating an ideal unfaulted sequence.

DISCUSSION

From crystal chemical study (Passaglia et al. 1998), the erionite structure accommodates a wider range of chemical variability, in terms of Si/Al ratio and extraframework cation content, than does offretite. The crystal chemical role of Mg is crucial, as the value of about 0.8 Mg atoms per cell (based on 72 framework O atoms) is the upper limit found in erionite minerals, whereas all offretites investigated have Mg contents from 1.4 to 2.0 Mg atoms per cell (also based on 72 framework O atoms for comparison). We can formulate a structural interpretation of the crystal-chemical role of Mg, based on the structural models obtained in the present investigation. In erionite, the largest channels are the eight-membered rings shared by two erionite cages. The average chemical content of two adjacent cages must be the same, and Ca-Mg repulsion, which is the basis of the extraframework cation distribution among the possible sites, limits the possible Mg locations in the cage. The large-radius Ca cation is the prevalent species in erionite, and it is more flexible than Mg in fulfilling the charge balance with the framework, because it can easily bond to framework O atoms and H_2O molecules in distorted sixfold, sevenfold, or higher coordination. The Mg ion seldom has a coordination different than octahedral, and given its small radius cannot form bonds with framework O atoms: No Mg-framework oxygen bonds are known in natural or synthetic zeolites. Therefore the erionite structure is limited in its ability to accommodate Mg. In offretite, the extraframework cations find extra space for geometrical arrangement in the large open channels delimited by the 12-membered rings of tetrahedra. The octahedrally coordinated Mg cations fit nicely in the gmelinite cage, and a substantial amount of Ca cations needed for framework charge compensation can be hosted in the open channels.

Thus, the ability of offretite to host a large amount of Mg is related to the presence of more than one type of large opening and therefore to the wider range of extraframework sites available. This model implies that the extraframework cations exert subtle control on the crystallization process by analogy with the model of the crystallization process in synthetic erionites and offretites, wherein the type and ratio of available cations controls the zeolite species crystallizing and the Si/Al ratio in the products (Lillerud and Raeder 1986).

This qualitative interpretation can also explain the segregation of Al in the erionite T2 tetrahedral sites. Charge compensation for the erionite T1 sites can only be derived

from cations hosted in the hexagonal prisms (which are empty), or from the cancrinite cage (containing only monovalent K cations). On the other hand, the T2 sites are charge compensated by the divalent cations in the erionite cage, and of course a better charge balance can be reached if Al is preferentially hosted in these sites. In offretite, not only can the divalent cations in the gmelinite cage compensate for Al on the T2 sites, and the monovalent cations in the cancrinite cage can compensate for Al on the T1 sites, but the cations in the large channels also contribute to charge compensation on both the T1 and T2 sites, allowing unrestricted distribution of Al on tetrahedral framework sites.

The results of the structural study support the crystal-chemical model proposed for the interpretation of the chemical data (Passaglia et al. 1998), that is, in the structure of erionite Mg can be hosted in the large erionite cage up to 0.8 Mg atoms per cell. Higher Mg contents are incompatible with the required amount of Ca cations in the erionite cavities, and the offretite-type structure is stabilized, possibly with the formation of erionite-offretite defect sequences.

Erionite-offretite intergrowths are probably much less common that previously thought in natural samples and seem to be restricted to samples at the high-Mg limit of the erionite field, as indicated by our TEM investigation. Although it is beyond the scope of this paper, mixed-phase samples may possibly be identified by X-ray powder diffraction from intensity ratios of the Bragg peaks. In this respect, the Rietveld method is of a straightforward and sophisticated technique for phase identification and quantification. The presence of structural disorder may result in a troublesome refinement, as shown in the case of the Araules erionite. An alternative and perhaps more appropriate technique for the characterization of structures with a high density of planar faults is the use of the interference function between structural layers. The program DiffaX (Treacy et al. 1991) can be successfully utilized for such calculations, as it has been recently shown by Treacy et al. (1996) also in the erionite-offretite case.

Acknowledgments

This research was supported under contract DE-AC02-76CH00016 with the Dept. of Energy by its Division of Chemical Sciences, Office of Basic Energy Sciences. A. Gualtieri was awarded a travel grant from the Fulbright U.S.A.-Italy Cultural Exchange Commission. Support is acknowledged from Italian MURST and CNR. H. Foy kindly made mineral samples available for the investigation. A. Alberti and D.L. Bish are thanked for useful suggestions and revision of the manuscript.

References cited

Alberti, A. and Gottardi, G. (1988) The determination of the Al-content in the tetrahedra of framework silicates. Zeitschrift für Kristallographie, 184, 49–61.

Alberti, A., Martucci, A., Galli, E., and Vezzalini, G. (1997) A reexamination of the crystal structure of erionite. Zeolites, 19, 349–352.

Alberti, A., Cruciani, G., Galli, E., and Vezzalini, G. (1996) A re-examination of the crystal structure of the zeolite offretite. Zeolites, 17, 457–461.

Amemiija, Y. (1990) Imaging plates-X-ray area detector based on photostimulable phosphor. Synchrotron Radiation News, 2, 21–26.

Artioli, G. and Kvick, Å. (1990) Synchrotron X-ray Rietveld study of perlialite, the natural counterpart of synthetic zeolite-L. European Journal of Mineralogy, 2, 749–759.

Barrer, R.M. and Villiger, H. (1969) The crystal structure of the synthetic zeolite-L. Zeitschrift für Kristallographie, 128, 352–370.

Batiashvili, T.V. and Gvakhariya, G.V. (1968) Erionite found for the first time in Georgia. Doklady Academii Nauk SSSR, 179, 122–124.

Belitsky, I.A. and Bukin, G.V. (1968) First find of erionite in the USSR. Doklady Academii Nauk SSSR, 178, 103–106.

Bennett, J.M. and Gard, J.A. (1967) The non-identity of the zeolites erionite and offreretite. Nature, 214, 1005–1006.

Bennett, J.M. and Grose, R.W. (1978) Characterization of the offretite-levynite intergrowth from Beech Creek, Oregon, by absorption and electron diffraction. In L.B. Sand and F.A. Mumpton, Eds., Natural Zeolites Occurrence, Properties, Use, p. 77–83. Pergamon Press, Oxford.

Fischer, R.X. (1996) Divergence slit corrections for Bragg-Brentano diffractometers with rectangular sample surface. Powder Diffraction, 11, 17–21.

Gard, J.A. and Tait, J.M. (1972) The crystal structure of the zeolite offretite $K_{1.1}Ca_{1.1}Mg_{0.7}[Si_{12.8}Al_{5.2}O_{36}]\times 15.2H_2O$. Acta Crystallographica, B28, 825–834.

———(1973) Refinement of the crystal structure of erionite. Proceedings of the 3rd International Conference on Molecular Sieves, p. 94–99. University Press, Leuven.

Gottardi, G. and Galli, E. (1985) Natural Zeolites. Springer-Verlag, Heidelberg, Germany.

Gualtieri, A., Norby, P., Hanson, J.C., and Hriljac, J. (1996) Rietveld refinement using synchrotron X-ray powder diffraction data collected in transmission geometry using an imaging plate detector: Application to standard m-ZrO_2. Journal of Applied Crystallography, 29, 707–713.

Gude, A.J. and Sheppard, R.A. (1981) Woolly erionite from the Reese River zeolite deposit, Lander County, Nevada, and its relationship to other erionites. Clays and Clay Minerals, 29, 378–384.

Hastings, J.B., Suortti, P., Thomlinson, W., Kvick, A., and Koetzle, T.F. (1983) Optical design for the NSLS crystallography beam line. Nuclear Instrumental methods, 208, 55–58.

Hill, R.J. and Gibbs, G.V. (1979) Variation in d(T-O), d(T..T) and TOT in silica and silicate minerals, phosphates and aluminates. Acta Crystallographica, B35, 25–35.

Kawahara, A. and Curien, H. (1969) La structure cristalline de l'érionite. Bulletin Societé Francaise Mineralogie Cristallographie, 92, 650–655.

Kerr, I.S., Gard, J.A., Barrer, R.M., and Galabova, I.M. (1970) Crystallographic aspects of the co-crystallization of zeolite L, offretite, and erionite. American Mineralogist, 55, 441–454.

Kokotailo, G.T., Sawruck, S., and Lawton, S.L. (1972) Direct observation of stacking faults in the zeolite erionite. American Mineralogist, 57, 439–444.

Larson, A.C. and Von Dreele, R.B. (1995) GSAS, General structure analysis system. Los Alamos National Laboratory, document LAUR 86–748.

Lillerud, K.P. and Raeder, J.H. (1986) On the synthesis of erionite-offretite intergrowth zeolites. Zeolites, 6, 474–483.

Matulis, C.E. and Taylor, J.C. (1992) Intensity calibration curves for Bragg-Brentano X-ray diffractometers. Powder Diffraction, 7, 89–94.

Millward, G.R., Ramdas, S., and Thomas, J.M. (1985) On the direct imaging of offretite, cancrinite, chabazite and other related ABC-6 zeolites and their intergrowth. Proceedings of the Royal Society of London, A 399, 57–71.

Mortier, W.J., Pluth, J.J., and Smith, J.V. (1976a) The crystal structure of dehydrated offretite with stacking faults of erionite type. Zeitschrift für Kristallographie, 143, 319–332.

———(1976b) Crystal structure of natural zeolite offretite after carbon monoxide absorption. Zeitschrift für Kristallographie, 144, 32–41.

Norby, P. (1997) Synchrotron powder diffraction using Imaging Plates: Crystal structure determination and Rietveld refinement. Journal of Applied Crystallography 30, 21–30.

Passaglia, E. and Tagliavini, A. (1994) Chabazite-offretite epitaxial over-

growths in cornubianite from Passo Forcel Rosso, Adamello, Italy. European Journal of Mineralogy, 6, 397–405.

Passaglia, E., Tagliavini, A., and Gutoni, R. (1996) Offretite and other zeolites from Fittà (Verona, Italy). Neues Jahrbuch für Mineralogie Monatschefte, 418–428.

Passaglia, E., Artioli, G., and Gualtieri, A. (1998) Crystal chemistry of the zeolites erionite and offretite. American Mineralogist, 83, 577–589.

Pongiluppi, D. (1976) Offretite, garronite and other zeolites from ''Central Massif'', France. Bulletin Societè Francaise Mineralogie et Cristallographie, 99, 322–327.

Schlenker, J.L., Pluth, J.J., and Smith, J.V. (1977) Dehydrated natural erionite with stacking faults of the offretite type. Acta Crystallographica, B33, 3265–3268.

Sheppard, R.A. and Gude, A.J. (1969) Chemical composition and physical properties of the related zeolites offretite and erionite. American Mineralogist, 54, 875–886.

Smith, J.V. and Bennett, J.M. (1981) Enumeration of 4-connected 3-dimensional nets and classification of framework silicates: the infinite set of ABC-6 nets; the Archimedean and σ-related nets. American Mineralogist, 66, 777–788.

Staples, L.W. and Gard, J.A. (1959) The fibrous zeolite erionite; its occurrence, unit cell, and structure. Mineralogical Magazine, 32, 261–281.

Treacy, M.M., Newsam, J.M., and Deem, M.W. (1991) A general recursion method for calculating diffracted intensities from crystals containing planar faults. Proceedings of the Royal Society of London, 433, 499–520.

Treacy, M.M., Higgins, J.B., and von Ballmoos, R. (1996) Collection of simulated XRD powder patterns for zeolites. Zeolites, 16, 323–802.

Wise, W.S. and Tschernich, R.W. (1976) The chemical compositions and origin of the zeolites offretite, erionite, and levyne. American Mineralogist, 61, 853–863.

Manuscript received March 31, 1997
Manuscript accepted December 14, 1997
Paper handled by Ronald C. Peterson